Controllability Limit of a Human Pilot

KYUICHIRO WASHIZU* AND KATSUYUKI MIYAJIMA†
University of Tokyo, Tokyo, Japan

The limit of a human pilot's capability in controlling an unstable second-order system, hereafter called an element, is theoretically analyzed; the transfer function of the human pilot is assumed, and the stability boundary of the closed system consisting of the human pilot and the controlled element is analyzed. The boundary thus obtained is considered to suggest the theoretical controllability limit of the human pilot. In connection with the theoretical analysis, fixed-base flight simulator tests are conducted; the analogous controlled element is set in the simulator, and the controllability limit is investigated by an experienced pilot. The physical interpretation of the experimental data with respect to the theoretical results shows good insight into the controllability limit of the human pilot.

Nomenclature

$Y_P(S)$	=	transfer function of human pilot
$Y_C(S)$	=	transfer function of control system
$Y_A(S)$	=	transfer function of controlled element
S	=	Laplace transform operator
K_P	=	human-pilot gain
K_C	=	control-system gain
K_A	=	controlled-element gain, 1/sec^2
K	=	closed-loop gain $K_PK_CK_A$, 1/sec^2
X	=	damping, rad/sec
Y	=	static stability, rad^2/sec^2
τ	=	reaction-time delay, sec
T_N	=	neuro-muscular lag, sec
T_L	=	lead, sec
T_I	=	lag, sec
ξ	=	output of control system
α	=	output of controlled element
ω	=	critical circular frequency of closed loop, rad/sec
T_2	=	time to double amplitude, sec

Introduction

AS a result of developments of V/STOL and high-speed flight vehicles, stability of a closed system consisting of an unstable object and a human pilot has become a subject of discussion. If the human pilot can control the object even if it has unstable characteristics, the object may be called controllable. Many papers concerning the limit of a human pilot's capability in controlling unstable objects have been presented.[1, 2]

This report is divided roughly into two parts. The first part is related to a theoretical analysis of a closed system consisting of an unstable element and a human pilot. The element is assumed to be represented by a second-order system as given by Eq. (1) where both static stability and damping may assume positive and negative values. The transfer function of a human pilot is assumed to be given by Eq. (3). The stability of the closed system is analyzed, and the limit of a human pilot's capability in controlling the unstable element is theoretically determined.

The second part is related to fixed-base simulator tests and comparisons of the test results with the theoretical predictions. In these tests, an experienced pilot controlled the element, the behavior of which is displayed on an oscilloscope. The limit of the pilot's capability has been experimentally determined by successive variations of damping as well as static stability. The theoretical results are compared with the results of the tests and those of Ref. 1, and show good insight into the controllability limit of the human pilot.

Received August 21, 1964; revision received January 11, 1965.

* Professor of Aeronautics. Member AIAA.
† Graduate student.

Theoretical Analysis

The block diagram of a closed system under consideration is shown in Fig. 1. The transfer function of the controlled element is assumed to be given by

$$Y_A(S) = K_A/(S^2 + XS + Y) \tag{1}$$

where K_A is a constant, and X and Y are the damping and static-stability terms, respectively. The element becomes unstable for negative values of X and/or Y. The transfer function of the control system is assumed to be given simply by

$$Y_C(S) = K_C \tag{2}$$

where K_C is a constant.

The transfer function of a human pilot is assumed to be expressed by the following equations[3–9]:

$$Y_P(S) = \frac{\text{pilot's force output}}{\text{pilot's visual input}} = \left\{\frac{e^{-\tau S}}{1 + T_NS}\right\}\left\{K_P\,\frac{1 + T_LS}{1 + T_IS}\right\} \tag{3}$$

The first factor in the right-hand side of Eq. (3), namely $e^{-\tau S}/(1 + T_NS)$, represents characteristics that are uncontrollable by the pilot. Its numerator and denominator represent a reaction-time delay and a neuro-muscular lag, respectively. The values of τ and T_N are considered to be about 0.10–0.30 sec and 0.1 sec, respectively. The second factor, namely $K_P(1 + T_LS)/(1 + T_IS)$, represents adjust-

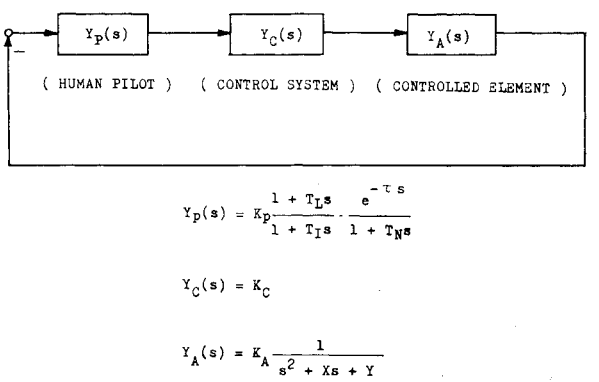

Fig. 1 Block diagram of the closed system.

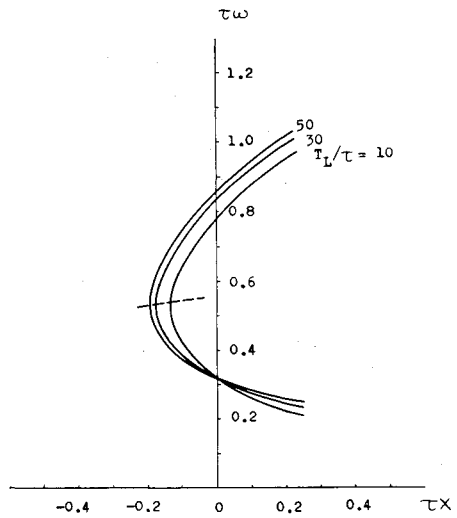

Fig. 2a Critical circular frequency at $\tau^2 Y = 0.10$.

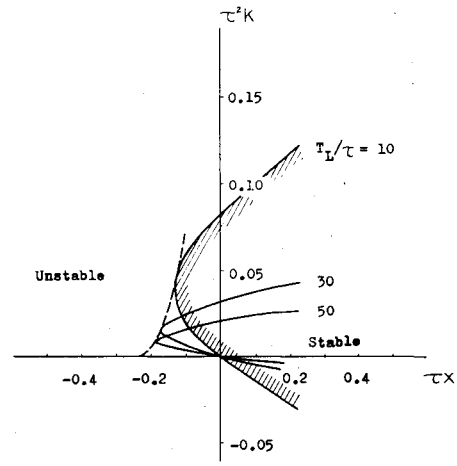

Fig. 2b Critical closed loop gain at $\tau^2 Y = 0.10$.

able characteristics. The human pilot can choose values of K_P, T_L, and T_I in a proper manner depending on the characteristics of the controlled element. In general, the values of T_L and T_I are considered to be around 0–5.0 and 0–20 sec, respectively. The upper limits of these two parameters have not been found yet. In addition to the transfer function described by Eq. (3), the pilot's output contains another portion called remnant, which is not expressed by a linear transfer function. However, the following analysis will not consider this portion of the pilot's output.

By employing the transfer functions thus assumed, it is now possible to study the stability characteristics of the closed system shown in Fig. 1. The characteristic equation of the closed loop is described by[10]

$$1 + Y_P(S) \cdot Y_C(S) \cdot Y_A(S) = 0 \tag{4}$$

A little consideration shows that the existence of a positive T_I in Eq. (3) fails to make the closed system more stable. Consequently, we may conclude that the pilot would try to make T_I as small as possible in controlling the element on the border between stability and instability, and we may assume the pilot's transfer function to be given by

$$Y_P(S) = K_P e^{-\tau S} \frac{1 + T_L S}{1 + T_N S} \tag{5}$$

in the following analysis. The characteristic equation (4) then becomes

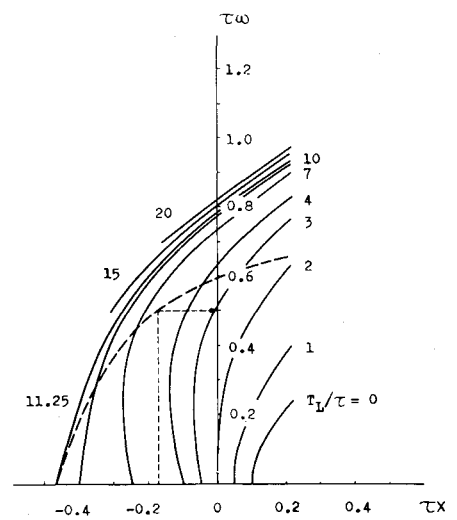

Fig. 3a Critical circular frequency at $\tau^2 Y = -0.05$.

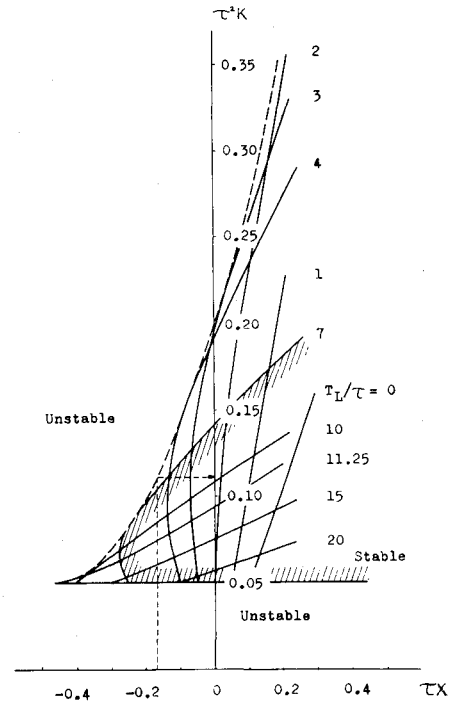

Fig. 3b Critical closed loop gain at $\tau^2 Y = -0.05$.

$$1 + Ke^{-\tau S} \frac{1 + T_L S}{1 + T_N S} \cdot \frac{1}{S^2 + XS + Y} = 0 \tag{6}$$

where

$$K = K_P K_C K_A \tag{7}$$

Equations that determine the stability boundary of the closed system can be obtained by putting $S = j\omega$ in Eq. (6), where $j = (-1)^{1/2}$, as follows:

$$\tan(\tau\omega) = \frac{(T_N T_L X - T_N + T_L)\omega^2 + X + (T_N - T_L)Y}{T_N T_L \omega^4 + \{1 + (T_N - T_L)X - T_N T_L Y\}\omega^2 - Y} \cdot \omega \tag{8}$$

$$K = \left[\frac{1 + T_N{}^2\omega^2}{1 + T_L{}^2\omega^2} \{(Y - \omega^2)^2 + X^2\omega^2\}\right]^{1/2} \tag{9}$$

Eqs. (8) and (9) determine the critical circular frequency ω and gain K on the stability boundary, respectively.

For the sake of simplicity in numerical analysis, we shall assume that the neuro-muscular lag T_N is equal to the reaction-time delay τ. Considering the order of magnitudes of these two parameters, this is believed to be an adequate simplification. Thus, we put

$$T_N = \tau \tag{10}$$

in subsequent analysis. Then Eqs. (8) and (9) reduce to the following equations:

$$\tan(\tau\omega) = \frac{-\{(\tau\omega)^2 - (\tau X + \tau^2 Y)\} + (T_L/\tau)\{(\tau X + 1)(\tau\omega)^2 - \tau^2 Y\}}{\{(\tau X + 1)(\tau\omega)^2 - \tau^2 Y\} + (T_L/\tau)\{(\tau\omega)^2 - (\tau X + \tau^2 Y)\}(\tau\omega)^2} \cdot (\tau\omega) \tag{11}$$

$$\tau^2 K = \left\{\frac{1 + (\tau\omega)^2}{1 + (T_L/\tau)^2(\tau\omega)^2}\left[\{\tau^2 Y - (\tau\omega)^2\}^2 + (\tau X)^2(\tau\omega)^2\right]\right\}^{1/2} \tag{12}$$

By solving Eqs. (11) and (12) simultaneously, we can determine the values of $\tau\omega$ and $\tau^2 K$ on the stability boundary. Typical results are shown for $\tau^2 Y = 0.10$ and -0.05 in Figs. 2 and 3, respectively. In these figures, the ordinates are $\tau\omega$ and $\tau^2 K$, the abscissa is τX, and T_L/τ appears as a parameter. The curves are the borders between stability and instability of the closed system. For example, the closed system is stable on the shaded sides for $T_L/\tau = 10$ and 7 in Figs. 2b and 3b, respectively. These figures show that for a set of τX, $\tau^2 Y$, and T_L/τ there exists for the value of $\tau^2 K$ a region that makes the closed system stable. Since a wider region means a wider margin for $\tau^2 K$, this region will be termed "gain margin" in this report. It is also observed that envelopes exist for the family of curves in Figs. 2b and 3b. The values of $\tau\omega$ corresponding to these envelopes are shown by broken lines in Figs. 2a and 3a.

Figures 2a and 2b show a case of positive static stability, $\tau^2 Y = 0.10$. It is observed from Fig. 2b that a large value of T_L/τ is desirable for the purpose of controlling a system with negative damping. However, a larger T_L/τ is accompanied by a smaller gain margin, which causes the human pilot difficulties in keeping the value of $\tau^2 K$ within the narrow band. Consequently, although the theory predicts that the controllability limit attained for the present case is $\tau X = -0.234$ for $T_L/\tau = +\infty$, such a state of zero gain margin can never be realized by the human pilot. Figures 3a and 3b show a case of negative static stability, $\tau^2 Y = -0.05$. It is seen from Fig. 3b that the lower boundary of the gain margin is limited by $\tau^2 K = 0.05$.

A controllability limit can now be obtained theoretically. For the region of positive static stability, theoretical values of $\tau^2 K$ and T_L/τ tend to zero and infinity, respectively, on the controllability limit. Consequently, the human pilot's transfer function on this limit reduces to

$$Y_P(S) = K_P^*[S/(1 + \tau S)]e^{-\tau S} \tag{13}$$

Thus the limit is obtained by a condition that Eq. (11) at $T_L/\tau = \infty$ has double roots with respect to ω^2. Employing an approximation that $\tan(\tau\omega) \cong \tau\omega$, which is equivalent to an approximation that $e^{-\tau S} \cong 1/(1 + \tau S)$ in Eq. (13), the critical circular frequency is given by

$$\tau\omega = (\tau^2 Y)^{1/4} \tag{14}$$

whereas the stable region is given as follows:

$$2\tau X \geq -\{1 - (\tau^2 Y)^{1/2}\}^2 \tag{15}$$

For the region of negative static stability, the limit is obtained by the conditions that Eq. (11) has double roots with respect to ω at $\omega = 0$, and Eq. (12) has double roots with respect to ω^2 at $\omega = 0$ when K is substituted by $-Y$. Thus we obtain

$$\tau X + 2\tau^2 Y - (T_L/\tau)\tau^2 Y = 0 \tag{16}$$

$$(\tau X)^2 + (\tau^2 Y)^2 - 2\tau^2 Y - (T_L/\tau)^2(\tau^2 Y)^2 = 0 \tag{17}$$

By solving these equations, we find that the critical T_L/τ is given by

$$T_L/\tau = 1.25 - 0.5/\tau^2 Y \tag{18}$$

and the stable region is given as follows:

$$4\tau X + 3\tau^2 Y \geq -2 \tag{19}$$

Equations (15) and (19) are shown in Fig. 4 for values of $\tau = 0.10$, 0.20, 0.30, and 0.40 sec.

Fixed-Base Simulator Tests

Simulator tests were conducted in order to find the validity of the theoretical analysis, using a fixed-base flight simulator consisting of an analog computer and a simulated cockpit. The block diagram of the test is the same as shown in Fig. 1 except that the value of K_A is taken equal to unity. The control system is a conventional stick with a weak spring that tends to restore the stick to the neutral position. The lateral movement of the stick was employed for the tests. The indicative system is an oscilloscope on which a vertical bright segment moves laterally.

Simulator tests were conducted by Y. Goto, an experienced pilot at National Aerospace Laboratory of Japan. To begin with, the bright segment was adjusted so that it was positioned at the center of the oscilloscope when no input was supplied. The controlled element in the computer was provided with negative damping and/or static stability. Then, an initial disturbance of an order of 0.4 cm was given to the segment, which began to move laterally and tended to diverge. The pilot was requested to return the segment to the center

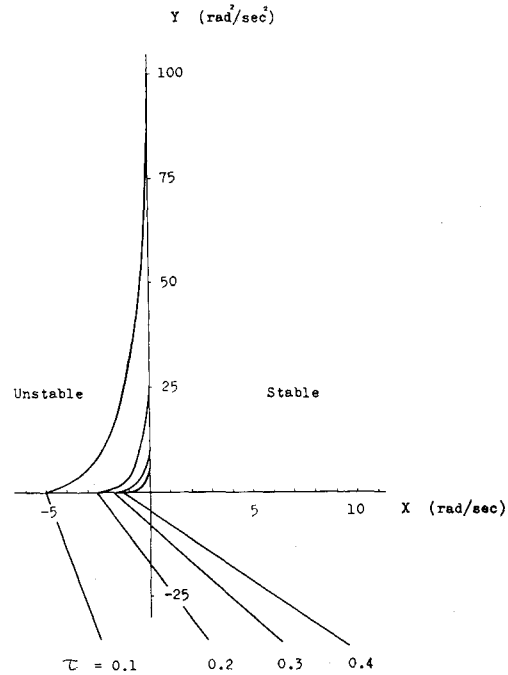

Fig. 4 Theoretical controllability limit.

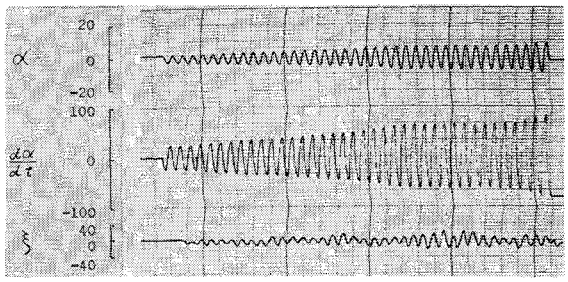

a) $Y = 100, X = -0.12$

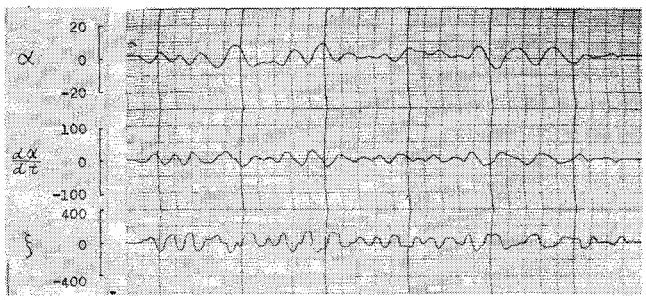

b) $Y = 0, X = -2.76$

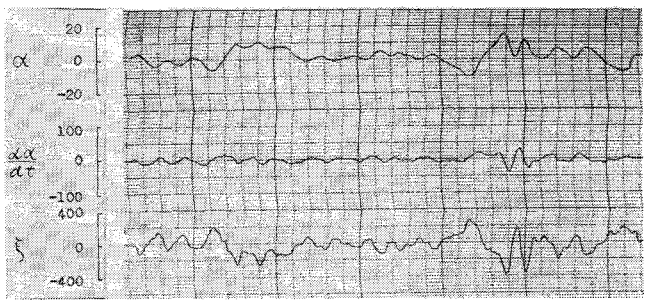

c) $Y = -15, X = -0.31$

Fig. 5 Piloting characteristics.

position and to keep the amplitude of the lateral movement within ±4 cm for 20 sec. In the tests, the value of static stability Y was varied step by step from 100 to −25, and the damping X was swept successively from positive to negative values for a fixed value of Y. When the pilot finds the system uncontrollable at one trial at a value of X for the first time during the sweep, this value of X was considered "the controllability limit at one trial" associated with the fixed value of Y. The test results are shown in Table 1.

Later, we wanted to find how the controllability limit could be improved by practicing, and allowed the pilot two more trials even if he failed at the first trial during the sweep.

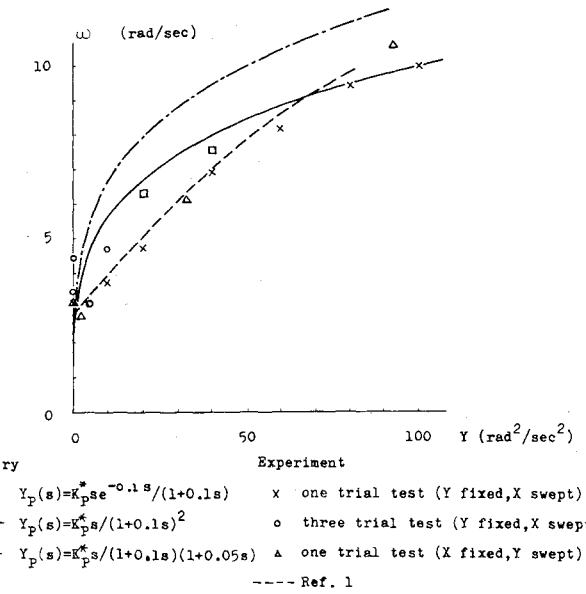

Fig. 6 Critical circular frequency for positive static stability.

If he could succeed in controlling the system within three trials, the system was considered within his controllability limit, and the pilot was requested to continue the sweep. Thus, we obtained "the controllability limit at three trials" associated with the fixed value of Y. The test was conducted by varying the value of Y in the sequence as shown in Table 2. It is observed from the table that the limit was improved by practicing, except in the first row for the case of $Y = 0$. This three-trial test was conducted two weeks after the one-trial test, so it seemed necessary for the pilot to take a few trials before he got accustomed again to the system. The second and subsequent rows indicated, evidently, the effect of practicing.

Furthermore, we wanted to find how the controllability limit might be influenced by the way of sweeping. This time, the value of damping X was varied in the sequence as shown in Table 3, and static stability Y was swept successively from zero to negative or positive values for a fixed value of X. When the pilot found the system uncontrollable at one trial at a value of Y for the first time during the sweep, this value of Y was considered the controllability limit at one trial associated with the fixed value of X. The test results, which are shown in Table 3, indicate that the controllability limit was not significantly influenced by the change of the way of sweeping for the controlled element of negative static stability, but was a bit improved for the controlled element of positive static stability.

Table 1 Typical results of one trial test (Y fixed, X swept)

Y, rad²/sec²	X, rad/sec	ω, rad/sec
100	−0.12	10.05
80	−0.12	9.42
60	−0.57	8.17
40	−1.14	6.91
20	−1.17	4.71
10	−1.16	3.77
5	−1.98	3.14
0	−2.47	3.14
−5	−1.68	3.14
−10.6	0	3.77
−15	0.78	4.40
−20	2.29	4.71
−25	4.09	5.03

Table 2 Typical results of three trial tests (Y fixed, X swept)

Y, rad²/sec²	X, rad/sec	ω, rad/sec
0	−2.15	3.46
5	−2.37	3.14
10	−2.60	4.71
5	−2.72	3.14
0	−2.85	4.40
−5	−2.21	4.08
−10	−0.91	4.40
−15	−0.31	3.77
−20	1.28	4.40
−25	2.11	3.77
−10	−1.47	3.77
0	−2.76	4.71

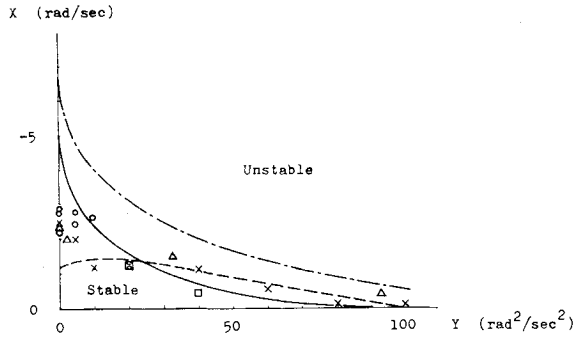

Fig. 7 Controllability limit for positive static stability.

Some typical records of the simulator tests are shown in Figs. 5a, 5b, and 5c. It is observed from these figures that the pilot relies on differential control when the controlled element is provided with a positive static stability, whereas he employs proportional control in a case of negative static stability, as expected from the theoretical analysis.

Comparison of Theory with Experimental Results

Figures 6 and 7 show representation of the theoretical and experimental results for positive values of static stability, where the static stability Y is an abscissa, and the critical value of the circular frequency ω and damping X are ordinates, respectively. The solid curves in these figures are plotted by solving Eqs. (14) and (15) for $\tau = 0.1$ sec. As mentioned previously, Eqs. (14) and (15) are derived under the assumption that $e^{-\tau s} \cong 1/(1 + \tau S)$, and the points marked by □ in these figures are obtained from the exact equation (11) to show the validity of the approximation. It is observed that the theoretical results are not in good agreement with the experimental results. This may suggest that Eq. (10) is not an adequate assumption on the controllability limit for a system with positive static stability. It seems very probable that, because the behavior of the controlled element has a definite periodicity for positive static stability even if it may diverge, the human pilot may be aware of the periodicity quickly and may perhaps succeed in reducing the value of τ to a smaller value. Keeping this in mind, Eqs. (14) and (15) are modified under the assumption that $e^{-\tau s} \cong 1/(1 + \tau S)$ to allow that T_N is different from τ. The result is as follows:

$$\tau\omega = \{\tau^2 Y/(T_N/\tau)\}^{1/4} \tag{20}$$

$$(\tau + T_N)X \geq -\{1 - (\tau T_N Y)^{1/2}\}^2 \tag{21}$$

Solutions of Eqs. (20) and (21) are obtained for $\tau = 0.05$ sec and $T_N = 0.10$ sec and are plotted in Figs. 6 and 7, respectively, with chain lines. These curves show that the reduction of the value of τ may be one of the important factors when the value of Y is considerably large.

Table 3 Typical results of one trial test (X fixed, Y swept)

X, rad/sec	Y, rad²/sec²	ω, rad/sec
5	−29.68	5.47
2	−22.92	4.71
0	−13.60	4.40
−0.5	−11.08	4.08
−1.0	−8.32	3.90
−1.5	−5.60	3.46
−2.0	−2.28	2.83
−2.29	0	3.14
−2.0	1.96	2.70
−1.5	32.60	6.09
−0.5	92.80	10.68

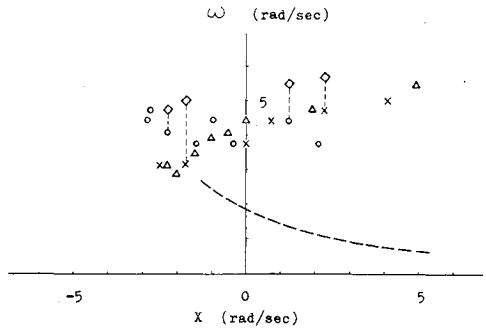

Fig. 8 Critical circular frequency for negative static stability.

Figures 8 and 9 show representation of the theoretical and experimental results for negative static stability, where the damping X is an abscissa, and the critical values of the circular frequency ω and static stability Y are ordinates, respectively, and the marks have the same meaning as those in Fig. 6. We have seen that at the theoretical controllability limit the critical circular frequency vanishes, and the relation between X and Y is given by Eq. (19). Thus the solid curve in Fig. 9 is plotted by solving Eq. (19) for $\tau = 0.1$ sec. It is observed that the theoretical results are not in good agreement with the experimental results. Some consideration will be given to this subject in the following paragraphs.

When the value of Y is negative, the controlled element has two real characteristic roots: one is positive and the other is negative. The instability of the element is mainly determined by the positive root, and the time to double amplitude, denoted by T_2, of the unstable root is related to the static stability Y and damping X as follows:

$$Y = -\{(\ln 2)/T_2\}[X + \{(\ln 2)/T_2\}] \tag{22}$$

These are a family of straight lines, as shown in Fig. 9, with T_2 as a parameter. It is observed from Fig. 9 that Eq. (22), when values of T_2 are taken equal to 0.240, 0.195, and 0.173 sec, is in good agreement with the experimental results obtained by Ref. 1 and with our experiments on one trial and on three trials, respectively, except for a region where the value of Y is nearly equal to zero. This may indicate that the human pilot controls the unstable element by taking notice of the unstable root only. However, in the region where the value of Y is nearly equal to zero, the damping of the mode corresponding to the negative root is small and the human pilot may be forced to take notice of both the stable and unstable roots. This may explain why the experimental results deviate from the corresponding straight lines in the vicinity of X axis.

As Fig. 3 indicates, the human pilot must keep values of $\tau^2 K$ and T_L/τ exactly constant at the theoretical controllability limit given by Eq. (19). This means that no margin is allowed for the two parameters at the limit. However,

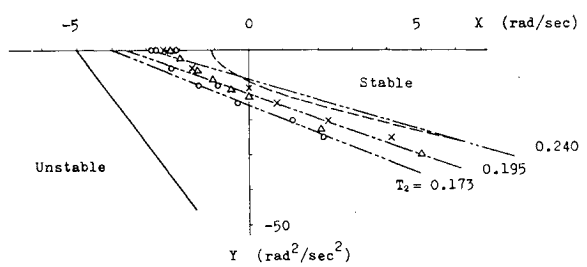

Fig. 9 Controllability limit for negative static stability.

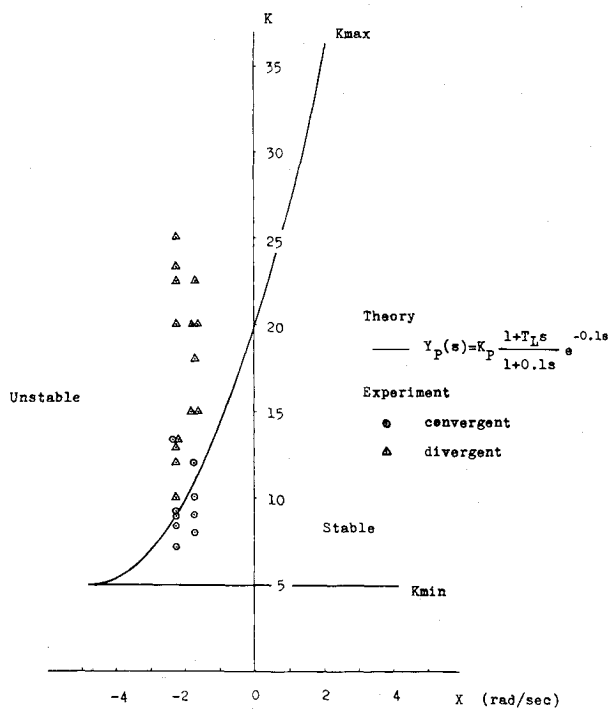

Fig. 10a Closed loop gain at $Y = -5$.

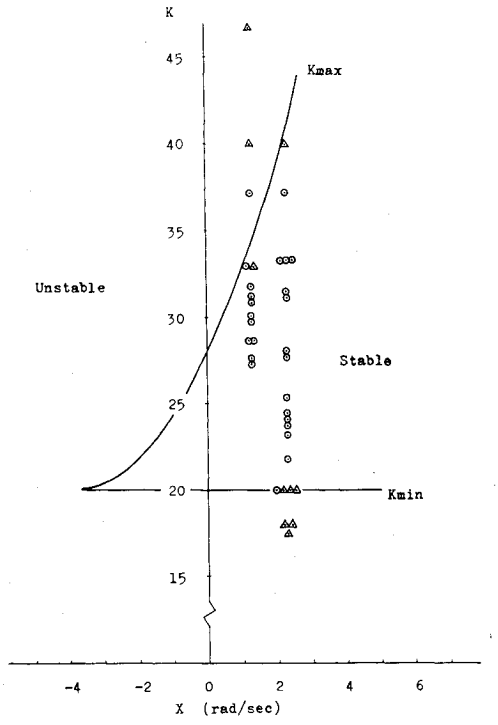

Fig. 10b Closed loop gain at $Y = -20$.

since it is impossible for him to keep these values exactly constant for such a long time as 20 sec, some gain margins should be allowed him. Consequently, his controllability limit may be narrower than the theoretical prediction. When a set of X, Y is given, he may perhaps adjust the value of T_L/τ so that maximum gain margin can be realized. With this in mind, we analyzed the experimental results to obtain Table 4, which is constructed as follows: to begin with, we assume that $\tau = 0.1$ sec; take a set of values of Y, X, and ω, such as -5, -1.68, and 3.14, from the controllability limit of the experiment (these correspond to $\tau^2 Y = -0.05$ and $\tau X = -0.168$ in Fig. 3); read values of K_{max} and K_{min} corresponding to $\tau X = -0.168$ from Fig. 3b, where K_{max} is given by the envelope of the curves, and K_{min} is obtained by the line $\tau^2 K = -\tau^2 Y$; read the value of T_L/τ corresponding to K_{max}; then, we can obtain the value of the critical circular frequency from the broken curve in Fig. 3a; finally, by using these values the first row of Table 4 can be completed, and the other three rows are completed in a similar manner.

In order to compare the values of K_{max} and K_{min} thus obtained with the experiments, values of the closed loop gain K were analyzed from the test results. Since the records of the tests seem to show repetitions of divergent, neutral, and convergent behaviors, only the extremal values of the output of the controlled element $\alpha_{extremal}$, and corresponding extremal values of the output of the control system $\xi_{extremal}$, were read out from the figures, and the values of K were calculated approximately by

$$K \cong -\xi_{extremal}/\alpha_{extremal} \tag{23}$$

The results are plotted in Figs. 10a and 10b and are compared with the theoretical results. In these figures, marks ⊙ and △ indicate that the output of the controlled element showed convergent and divergent behavior, respectively, at the instant when the value of α was read out. It is observed that, if this interpretation of the experimental data is employed, the theoretical results show good insight into the pilot behavior.

Concerning the critical circular frequencies listed in Table 4, we note that the critical frequencies obtained experimentally are not always very clearly noticeable from the test records, as observed from Figs. 5b and 5c. The critical frequencies obtained theoretically and experimentally are plotted in Fig. 8 and marked with ◇, and × or ○, respectively. The corresponding critical frequencies are connected by dotted lines.

It is interesting to observe from Table 4 that the ratio K_{max}/K_{min} seems to take nearly constant value for each trial test. This might suggest that the ratio of K_{max}/K_{min} may be one of the decisive factors as the criterion of gain margin for the human pilot on the threshold of instability, although a more general criterion may be expressed such that

$$f(\tau^2 K_{max}, \tau^2 K_{min}, T_L/\tau, \tau X, \tau^2 Y) = 0 \tag{24}$$

To emphasize this circumstance, values of K_{max}/K_{min} are calculated for several sets of (X, Y) on the straight lines with the constant times to double amplitude shown in Fig. 9. The calculations have been made for the straight lines indicating $T_2 = 0.195$ and 0.173 sec, respectively, and the results are shown in Table 5. It is seen that the condition that the time to double amplitude is constant seems roughly to correspond to the condition that K_{max}/K_{min} is constant.

Final Remarks

It may be mentioned from the analysis and experiments that the proposal of representing the transfer function of a human pilot by Eq. (1), and of employing the characteristic equation of the closed system, Eq. (4), seems to provide one of the clues for the analysis of the controllability limit of the human pilot. It may be added that results of analyses of this kind can be fed to the human pilot so that he can realize a better technique for widening his controllability limit.

References

[1] Taylor, L. W., Jr. and Day, R. E., "Flight controllability limits and related human transfer functions as determined from simulator and flight tests," NASA TN D-746 (May 1961).

[2] Sadoff, M., McFadden, N. M., and Heinle, D. R., "A study of longitudinal control problems at low and negative damping and stability with emphasis on effects of motion cues," NASA TN D-348 (January 1961).

Table 4 Gain margin and critical circular frequency

Test (Y fixed, X swept)	Experiment Y, rad²/sec²	X, rad/sec	ω, rad/sec	Theory K_{max}	K_{min}	ω, rad/sec	K_{max}/K_{min}
One trial	−5	−1.68	3.14	11.2	5	5.0	2.24
	−20	2.29	4.71	41.4	20	5.7	2.07
Three trials	−5	−2.21	4.08	9.4	5	4.7	1.88
	−20	1.28	4.40	33.8	20	5.5	1.69

Table 5 Gain margin and time to double amplitude

T_2	Y, rad²/sec²	X, rad/sec	K_{max}	K_{min}	K_{max}/K_{min}
0.195	−5	−2.14	9.60	5	1.92
	−20	2.08	39.20	20	1.96
0.173	−5	−2.75	7.50	5	1.50
	−20	1.00	32.40	20	1.62

[3] Westbrook, C. B., "Handling qualities and pilot dynamics," Aerospace Eng. **18**, 26–32 (May 1959).

[4] Tustin, A., "The nature of the operator's response in manual control and its implications for controller design," J. Inst. Elec. Engrs. (London) **94**, 190–202 (1947).

[5] Ashkenas, I. L. and McRuer, D. T., "A theory of handling qualities derived from pilot-vehicle system considerations," Aerospace Eng. **21**, 60–61, 83–102 (February 1962).

[6] McRuer, D. T. and Krendel, E. S., "The human operator as a servo system element, Part I," J. Franklin Inst. **267**, 381–403 (1959).

[7] McRuer, D. T. and Krendel, E. S., "The human operator as a servo system element, Part II," J. Franklin Inst. **267**, 511–536 (1959).

[8] Hall, I. A. M., "Study of the human pilot as a servo-element," J. Royal Aeron. Soc. **67**, 351–360 (June 1963).

[9] Chattler, L. M., "The human pilot," Northrop Aircraft, Inc., Bureau of Aeronautics Rept. AE-61-4III (August 1954).

[10] Brown, G. S. and Campbell, D. P., *Principles of Servomechanisms* (John Wiley & Sons, Inc., New York, and Chapman & Hall, Ltd., London, 1958).

MAY 1965 AIAA JOURNAL VOL. 3, NO. 5

A Thermal Vacuum Technique for Measuring the Solar Absorptance of Satellite Coatings as a Function of Angle of Incidence

MARLA G. HOKE*
NASA Goddard Space Flight Center, Greenbelt, Md.

An experimental technique for measuring the solar absorptance of a satellite coating as a function of angle of incidence has been developed. A thermal vacuum method is used to measure the equilibrium temperature of a coated sample as the sample is turned with respect to the incident beam by means of a rotational apparatus installed in the vacuum chamber. Preliminary measurements of the directional solar absorptance of the following materials have been made: evaporated aluminum, evaporated gold, aluminum leafing paint, zinc sulfide paint, and Parson's black paint. The hemispherical solar absorptance is calculated for evaporated aluminum.

Introduction

A FUNDAMENTAL problem in the analysis and design of temperature-controlled spacecraft is the prediction of the equilibrium temperature of the satellite in orbit. In order to solve the radiation balance equation for the equilibrium temperature of a satellite, the solar absorptances of the spacecraft surfaces are usually required. Because of the surface geometry of the satellite, its surfaces usually do not lie perpendicular to the incident sun illumination. Therefore, it is of fundamental importance to know the solar absorptance of a coating as a function of angle of incidence.

The average solar absorptance of a coating can be measured by knowing the equilibrium temperature of the sample coating when suspended in an evacuated chamber and illuminated by a source whose spectral distribution is similar to that of the sun. A rotating frame apparatus was designed which allows a sample, placed in the frame, to be turned to different angles with respect to the incident illumination. Since a gear coupling was employed to rotate the frame, a calibration technique, using the optical method of superposition of reflected and incident parallel beams, was devised in order to determine the true angular position of the sample.

Directional solar absorptances of the following materials have been measured: evaporated aluminum, evaporated gold, aluminum leafing paint, zinc sulfide paint, and Parson's black paint. Curves obtained from these data appear to agree well with theoretical expectations based on the Fresnel equations. The evaporated aluminum data was used to illustrate the calculation of the surface-average solar absorptance for a sphere.

Received July 30, 1964; revision received February 16, 1965.

* Aerospace Engineer, Coatings Section, Thermal Systems Branch.

Rotational Apparatus

Design and Alignment of Sample Holders and Support Shafts

The apparatus designed for this experiment consists of two sample holders and the hardware necessary for adapting the